iScience

CellPress
OPEN ACCESS

Article

GATA1 deletion in human pluripotent stem cells increases differentiation yield and maturity of neutrophils

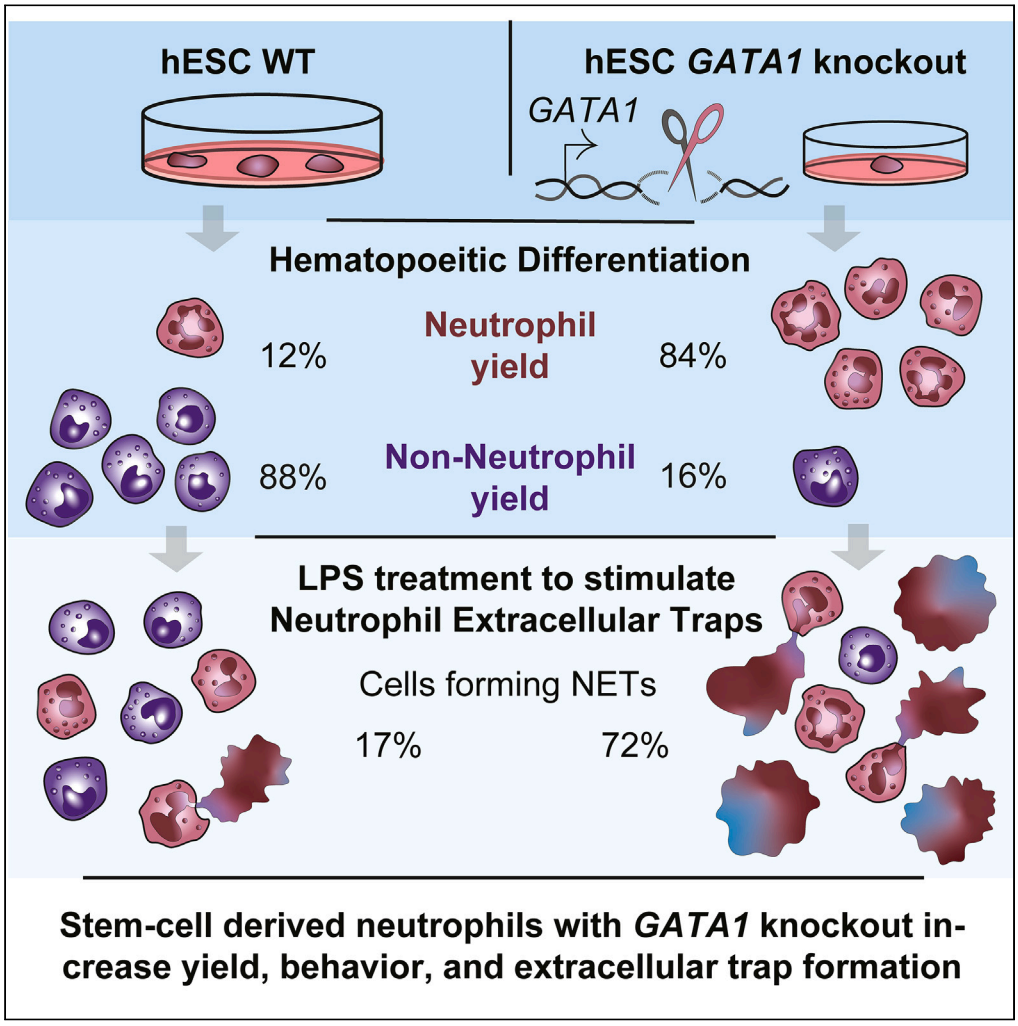

Thomas C. Harper, Elaine M. Oberlick, Tomas J. Smith, ..., Corey D. Driscoll, Sarah F. Mowbray, Christophe Antczak

tomdomma@gmail.com

Highlights

hPSCs with *GATA1* deletion generate highly enriched and mature iNeutrophils

GATA1 KO iNeutrophils retain their host defense functions

Unlike WT iNeutrophils, *GATA1* KO iNeutrophils produce NETs after LPS stimulation

GATA1 KO iNeutrophils are a powerful tool to validate NET targets using CRISPR-Cas9

Harper et al., iScience *26*, 107804
October 20, 2023
https://doi.org/10.1016/j.isci.2023.107804

iScience

CellPress
OPEN ACCESS

Article

GATA1 deletion in human pluripotent stem cells increases differentiation yield and maturity of neutrophils

Thomas C. Harper,[1,3,*] Elaine M. Oberlick,[2] Tomas J. Smith,[2] Duncan E. Nunes,[2] Mark-Anthony Bray,[1] Seonmi Park,[1] Corey D. Driscoll,[2] Sarah F. Mowbray,[2] and Christophe Antczak[1]

SUMMARY

Human pluripotent stem cell (hPSC)-derived tissues can be used to model diseases in cell types that are challenging to harvest and study at-scale, such as neutrophils. Neutrophil dysregulation, specifically neutrophil extracellular trap (NET) formation, plays a critical role in the prognosis and progression of multiple diseases, including COVID-19. While hPSCs can generate limitless neutrophils (iNeutrophils) to study these processes, current differentiation protocols generate heterogeneous cultures of granulocytes and precursors. Here, we describe a method to improve iNeutrophil differentiations through the deletion of *GATA1*. *GATA1* knockout (KO) iNeutrophils are nearly identical to primary neutrophils in form and function. Unlike wild-type iNeutrophils, *GATA1* KO iNeutrophils generate NETs in response to the physiologic stimulant lipopolysaccharide, suggesting they are a more accurate model when performing NET inhibitor screens. Furthermore, through deletion of *CYBB*, we demonstrate that *GATA1* KO iNeutrophils are a powerful tool in determining involvement of a given protein in NET formation.

INTRODUCTION

Neutrophils are the most abundant immune cells in the human body and make up approximately 70% of circulating leukocytes. They migrate to the site of infections where they recruit other immune cells and independently destroy invading microorganisms through phagocytosis, the release of granules, and the formation of neutrophil extracellular traps (NETs).[1,2]

While neutrophils are an important first line of defense in the innate immune system, their overactivation can have a proportionally negative impact on many diseases and affect numerous organ systems. The dysregulation of neutrophils is correlated with the progression of multiple diseases including rheumatoid arthritis, atherosclerosis, psoriasis, chronic obstructive pulmonary disease, and gallstone formation.[3–7]

COVID-19 clearly establishes the link between overactive neutrophils and disease severity and highlights the need for improved methods to model neutrophil dysregulation. Severe acute respiratory syndrome coronavirus 2, the virus which causes COVID-19, has been shown to directly induce NETs[8,9] and the overproduction of NETs and neutrophil reactive oxygen species (ROS) exacerbates COVID-19 complications including blood clots, cytokine storm, organ damage, and respiratory failure.[10–13] Unsurprisingly, there is a strong positive correlation between NET production, disease severity, and patient outcome.[14,15]

While inhibiting overactive neutrophils has the potential to mitigate COVID-19 severity,[15–17] the nature of primary neutrophils severely restricts their utility in drug discovery. Primary neutrophils, like all donor tissues, are limited by access and cross-patient variability, survive *ex vivo* for less than 24 h, are transcriptionally silent and non-proliferative, and cannot be cryopreserved.[18] These shortcomings preclude large-scale drug screening and make unbiased genetic screens and target validation experiments using CRISPR-Cas9 challenging.

Human pluripotent stem cells (hPSCs) provide an inexhaustible source of material that can overcome these challenges. hPSCs self-renew indefinitely, can be differentiated into a variety of highly relevant cell types, and are easy to genetically modify. hPSC-derived cells have been successfully used in a variety of pharmaceutical efforts, ranging from high-throughput phenotypic drug screens to model and correct neurological disorders, to the generation of hepatocytes to screen drug-mediated toxicity.[19,20] The production of homogeneous cultures of mature cells is crucial for assay relevance and reproducibility. Unfortunately, current protocols to produce hPSC-derived limitless neutrophils (iNeutrophils) generate a heterogeneous combination of hematopoietic progenitors and cells resembling neutrophils, eosinophils, and basophils.[21–25]

Neutrophil specification is tightly regulated by an interplay of cell fate-determining transcription regulators. While eosinophils and neutrophils rely on the expression of *CEBPE* and *GFI1*, posttranslational acetylation of CEBPE at K121 and K127 along with the reduction of *GATA1*

[1]Chemical Biology and Therapeutics, Novartis Institutes for BioMedical Research, Cambridge, MA, USA
[2]Respiratory Disease Area, Novartis Institutes for BioMedical Research, Cambridge, MA, USA
[3]Lead contact
*Correspondence: tomdomma@gmail.com
https://doi.org/10.1016/j.isci.2023.107804

ultimately determines neutrophil commitment.[26,27] During neutrophil maturation, *CEBPE* is downregulated and expression of the terminal granulopoiesis genes *CEBPD* and *SPI1* escalates.[28] The small molecules and cytokines governing these events are largely unknown. Based on transcriptional analysis of sorted iNeutrophils along with mouse genetic studies, we surmised that the deletion of *GATA1*, a transcription factor important for the development of eosinophils and basophils, would guide hPSC-derived granulocytes into a neutrophil-specific program and eliminate contaminating cells.[29,30] We demonstrate that knocking out *GATA1* in H1 human embryonic stem cells (hESCs) using CRISPR-Cas9 (*GATA1* knockout (KO)) followed by granulocyte differentiation produces highly enriched populations of iNeutrophils that are nearly identical to their primary counterparts. Compared to wild-type (WT) iNeutrophils, *GATA1* KO iNeutrophils have dramatically improved levels of the neutrophil surface markers CD182, CD11b, CD15, CD16, and CD66b and retain their host defense functions including phagocytosis, ROS production, and myeloperoxidase (MPO) activity. Unlike WT iNeutrophils, *GATA1* KO iNeutrophils form significant NETs after treatment with the physiologic NET-stimulant lipopolysaccharide (LPS). Furthermore, *GATA1* KO iNeutrophils can be further genetically manipulated through CRISPR-Cas9 to evaluate the role of individual genes in neutrophil functions. *GATA1* KO iNeutrophils with deletion of *CYBB*, which encodes a protein involved in NET formation, produce reduced NETs in response to the NET-stimulant phorbol myristate acetate (PMA).

RESULTS

Conventional cytokine differentiation yields heterogeneous iNeutrophils

First, we generated hemogenic endothelium using cytokines and small molecules following previously published protocols[31,32] (Figures 1A and 1B). Next, we supplemented the hematopoietic progenitor's media with granulocyte colony-stimulating factor (G-CSF) to further differentiate the cells toward a neutrophil lineage.[33] Hematoxylin and eosin images of Day 19 iNeutrophils revealed a variety of cell types with morphologies consistent with different granulocytes and progenitors (Figure 1C). Flow cytometry analysis identified two major populations distinguishable by size (forward-scatter) and granularity (side-scatter) (Figure 1D). The larger, more granular cells expressed high levels of the non-neutrophil granulocyte surface markers Siglec-8 and CD193, while the smaller, less granular cells expressed high levels of the neutrophil surface markers CD15 and CD16. These smaller, less granular cells also expressed lower levels of the hematopoietic progenitor marker CD33 and higher levels of the mature granulocyte marker CD66b, suggesting this population is immunophenotypically like mature neutrophils. As expected, the pan-hematopoietic marker CD45 was similar in both populations of floating cells (Figures 1E and 1F).

Next, we sorted the low and high forward- and side-scatter populations using FACS and compared the transcript levels of five regulators of granulocyte specification. While most regulators had a 5-fold difference or less in transcript levels between the two groups, *GATA1* was upregulated more than 25-fold in the non-neutrophil population (Figure 1G). Studies in mice demonstrate that *Gata1* is critical in the development of eosinophils and basophils, and while it is expressed in the common myeloid progenitor, it is dispensable for the differentiation and function of neutrophils.[29,30] Additionally, mature circulating neutrophils do not express *Gata1*, and the deletion of *Gata1* in adult mice severely reduces the number of eosinophils while increasing neutrophils.[34] These findings suggest that *GATA1* is a key gene responsible for specifying the non-neutrophil population and downregulation could promote the desired neutrophil fate.

GATA1 KO improves iNeutrophil specification and maturation

We devised a novel differentiation approach by deleting *GATA1* in our hESCs to promote the desired neutrophil cell type. Like their WT counterparts, *GATA1* KO hESCs were able to self-renew and expressed high levels of the pluripotency markers *OCT4* and *NANOG* (Figure 2A). Upon differentiation, both the WT and *GATA1* KO cells downregulated these pluripotency genes and began expressing the hematopoietic transcription regulators *SPI1* and *GFI1* (Figure 2B). By Day 12, the WT and *GATA1* KO hematopoietic progenitors showed differences in gene expression suggesting the *GATA1* KO cells were more neutrophil-like than the WT cells. The Day 12 *GATA1* KO hematopoietic progenitors expressed significantly higher levels of the neutrophil genes *AZU1*, *AQP9*, *ELANE*, and *MPO* and significantly lower levels of the eosinophil and basophil-specific gene *CLC* (Figures 2C and 2D).

Hematoxylin and eosin images of Day 19 *GATA1* KO iNeutrophils showed a dramatic increase in the number of cells with the classic neutrophil multilobulated nuclear morphology (Figures 2E and S3). Furthermore, the *GATA1* KO cells generated 20.8 $\pm$ 3.9 $\times$ 10^6 floating cells from the 6 $\times$ 10^4 hESCs plated into each 6 cm dish, roughly three times that of the WT cells (6.8 $\pm$ 0.8 $\times$ 10^6), demonstrating that this improved differentiation method can produce at-scale numbers of homogeneous iNeutrophils (Figure 2F).

GATA1 KO iNeutrophils share many characteristics of primary neutrophils

Surface proteins on immune cells mediate cell communication and signal transduction and are often used to distinguish different granulocytes. We used fluorophore-conjugated antibodies specific to basophil, eosinophil, and neutrophil surface proteins (Figure 3A) and flow cytometry to compare WT and *GATA1* KO iNeutrophils versus primary neutrophils. Staining WT iNeutrophils using antibodies against Siglec-8 showed that 51 $\pm$ 1% of the cells adopted an eosinophil phenotype, supported further by the co-expression of CD193 in 30 $\pm$ 5% of the total floating cells. Additionally, 29 $\pm$ 2% of the WT cells expressed the non-neutrophil granulocyte marker CD49d. Alternatively, 5 $\pm$ 1% of the *GATA1* KO iNeutrophils expressed Siglec-8 and 3 $\pm$ 1% co-expressed CD193. Only 8 $\pm$ 1% of the *GATA1* KO iNeutrophils expressed CD49d (Figures 3B, S4A, and S4B).

While 88 $\pm$ 5% and 76 $\pm$ 10% of the WT iNeutrophils expressed CD182 and CD11b, respectively, fewer were positive for the mature neutrophil markers CD15 (47 $\pm$ 3%) and CD16 (30 $\pm$ 1%), and only 20 $\pm$ 2% expressed the mature granulocyte marker CD66b. Alternatively, we saw a dramatic increase in not only the number of CD182 (95 $\pm$ 1%) and CD11b (97 $\pm$ 1%)-positive *GATA1* KO iNeutrophils but also in the

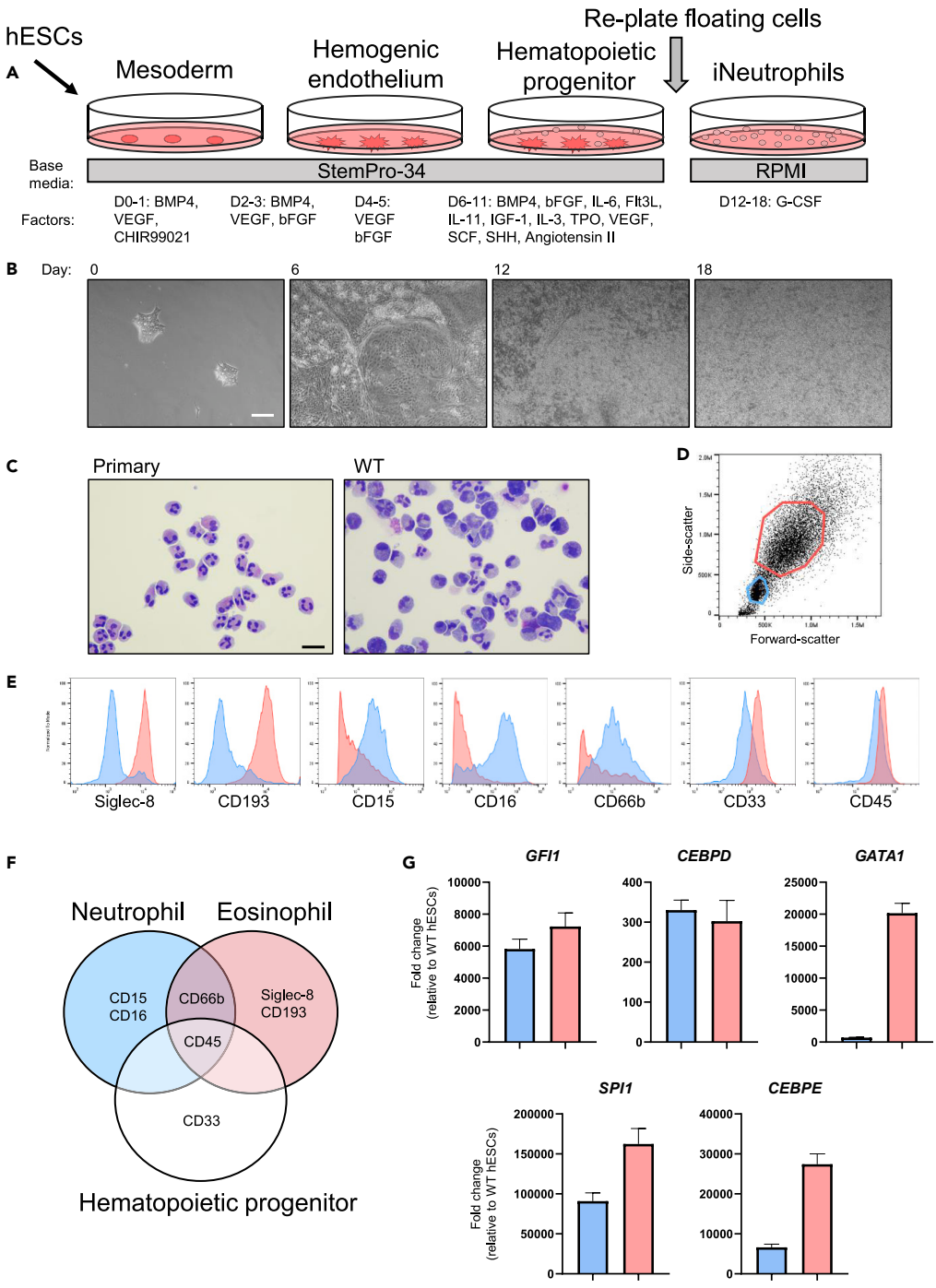

Figure 1. iNeutrophils generated using conventional differentiation methods are heterogeneous

(A) Schematic timeline of differentiation process including base media and soluble factor supplements.

(B) Bright-field images of differentiation at key time points. Scale bar, 100 μm.

(C) Hematoxylin and eosin images of iNeutrophils harvested on Day 19 compared to primary neutrophils. Scale bar, 20 μm.

(D) Flow cytometry scatterplot of iNeutrophils collected on Day 19. Red gate surrounds high forward- and side-scatter population and blue gate surrounds low forward- and side-scatter population.

(E) Flow cytometry analysis of blue and red gated populations from scatterplot.

(F) Venn diagram of neutrophil, eosinophil, and hematopoietic progenitor cell surface markers.

(G) RT-qPCR of *GFI1*, *CEBPD*, *GATA1*, *SPI1*, and *CEBPB* performed on blue and red gated populations from (E) after sorting using FACS. Data normalized to *GAPDH* (n = 1 independent experiment; mean ± SD of technical triplicates).

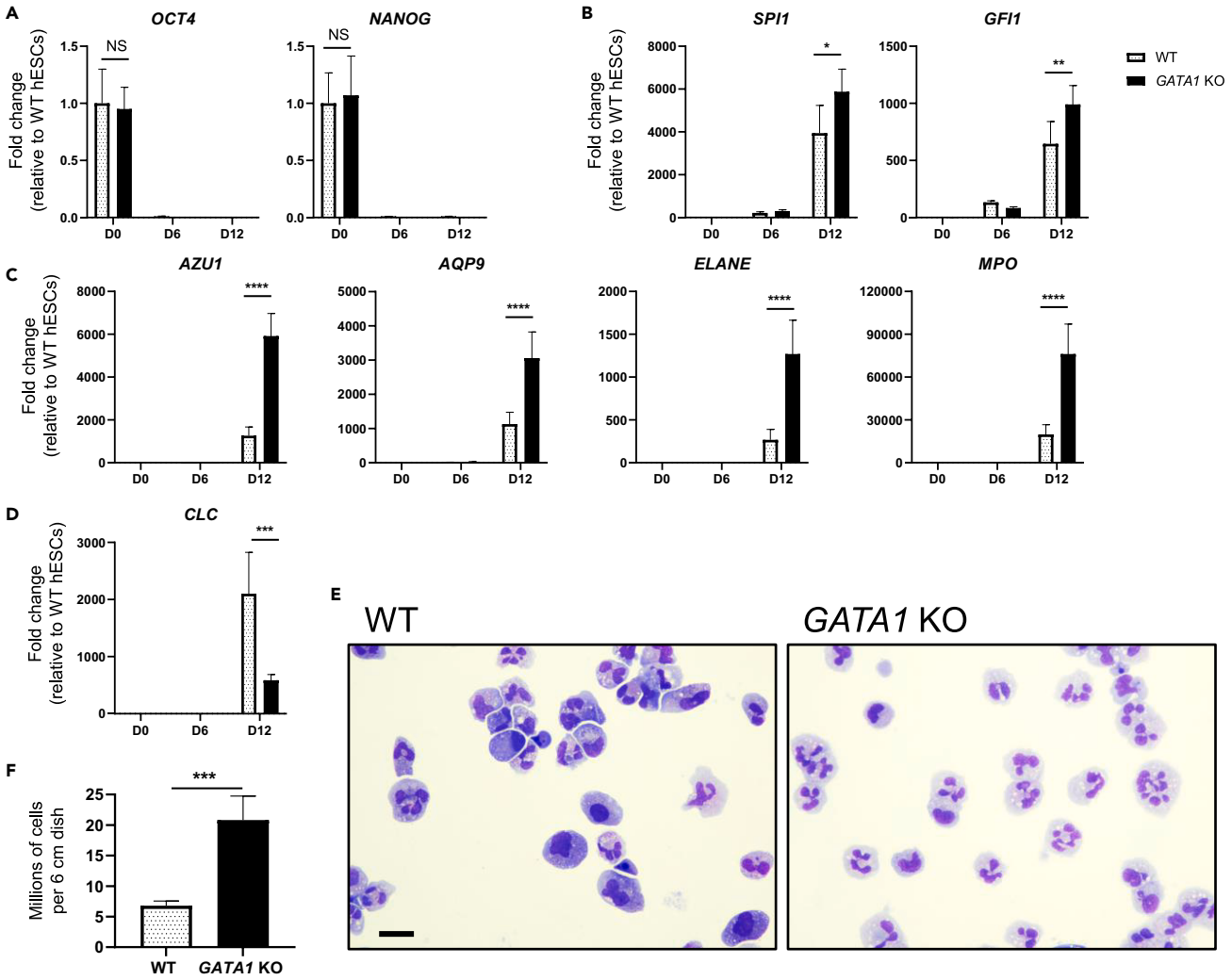

Figure 2. *GATA1* KO improves iNeutrophil gene expression and phenotype

(A–D) RT-qPCR of pluripotency genes *OCT4*, *NANOG*, (B) hematopoietic transcription regulators genes *SPI1*, *GFI1*, (C) neutrophil-specific genes *AZU1*, *AQP9*, *ELANE*, *MPO* (D), and the eosinophil and basophil gene *CLC* on Day 0, 6 and 12 of differentiation. Data are normalized to *GAPDH* and expressed as fold-change relative to WT hESCs (n = 3 independent experiments; mean ± SD). *p < 0.05, **p < 0.01 ***p < 0.001, ****p < 0.0001 determined by two-way ANOVA.

(E) Hematoxylin and eosin images of WT and *GATA1* KO iNeutrophils harvested on Day 19. Scale bar, 20 μm.

(F) Number of floating cells produced by WT and *GATA1* KO cultures in each 6 cm dish on Day 19 (n = 4 independent experiments; mean ± SD). ***p < 0.001 determined by unpaired t-test.

magnitude of signal. The percentage of CD15 (96 ± 1) and CD16 (93 ± 2)-positive cells were significantly higher in the *GATA1* KO iNeutrophils relative to WT iNeutrophils, and 92 ± 4% expressed CD66b (Figures 3C and S4C). Multiplexed staining revealed that 84 ± 2% of the *GATA1* KO iNeutrophils were co-positive for all of the neutrophil surface markers tested compared to only 12 ± 2% of the WT iNeutrophils (Figure S4D).

The *GATA1* KO iNeutrophils produced a homogeneous forward- and side-scatter profile which largely localized to the previously determined neutrophil-like cell population seen in WT cells (Figures 1D, 1E, and 3D). The diffuse, non-neutrophil-like population was dramatically reduced. Interestingly, the *GATA1* KO iNeutrophil population overlaps with the forward- and side-scatter profile seen in primary neutrophils (Figure 3D). Taken together, these results clearly show a remarkable similarity in surface protein expression, size, and granularity between the *GATA1* KO iNeutrophils and primary neutrophils.

GATA1 KO does not impact host defense functions

Neutrophils are a critical component of innate immunity and kill invading microorganisms through phagocytosis, MPO release, and ROS production. Analysis revealed that the *GATA1* KO iNeutrophils retained these important functions.

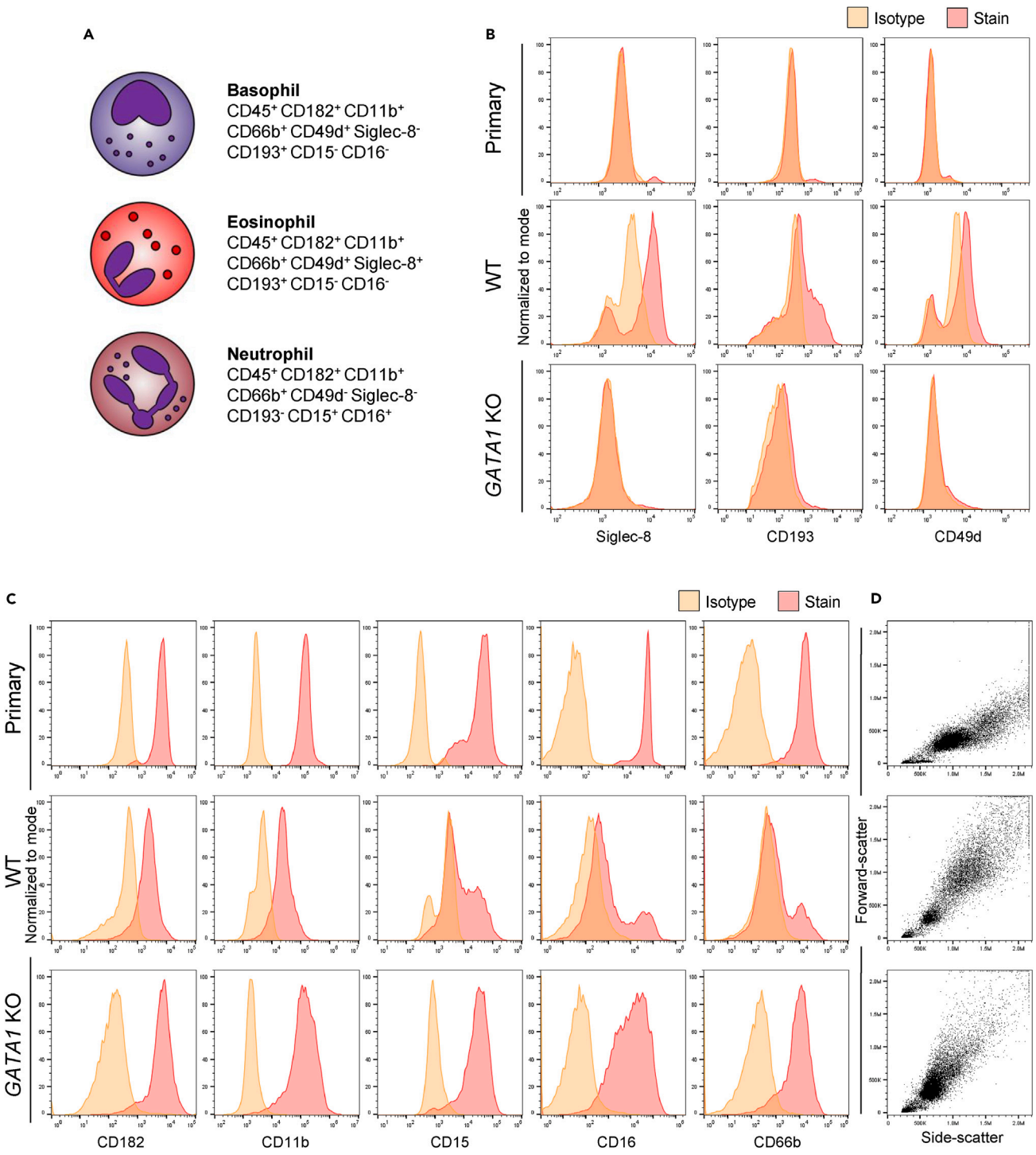

Figure 3. *GATA1* KO iNeutrophils are immunophenotypically like primary neutrophils

(A) Schematic summary of proteins expressed on basophils, eosinophils, and neutrophils.

(B and C) Flow cytometry analysis of primary neutrophils, WT, and *GATA1* KO iNeutrophils stained using antibodies against non-neutrophil granulocyte surface markers Siglec-8, CD193, and CD49d (C) and antibodies against neutrophil markers CD182, CD11b, CD15, CD16, and CD66b on Day 19. Plots show isotype control (orange) and corresponding specific antibody (red) histograms (representative data from n = 3 independent experiments and 1 independent donor).

(D) Flow cytometry generated forward- and side-scatter plots of primary neutrophils, WT, and *GATA1* KO iNeutrophils on Day 19 (representative data from n = 3 independent experiments and 1 independent donor).

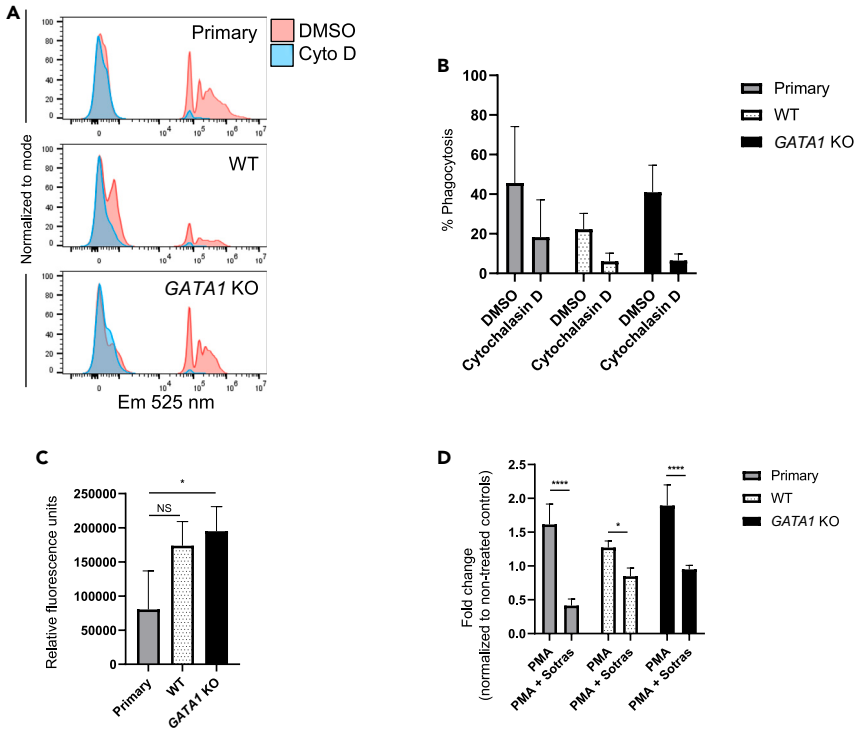

Figure 4. *GATA1* KO iNeutrophils retain critical host defense functions

(A and B) Histograms represent phagocytosis of opsonized fluorescent microspheres in primary neutrophils, WT, and *GATA1* KO iNeutrophils on Day 19 treated with DMSO (red) or 20 μM cytochalasin D (blue) along with (B) percentage uptake (n = 3 independent experiments and 3 independent donors; mean ± SD).

(C) Myeloperoxidase (MPO) activity tested via chlorination in primary neutrophils, WT, and *GATA1* KO iNeutrophils on Day 19 (n = 3 independent experiments and 3 independent donors; mean ± SD). *p < 0.05 determined by one-way ANOVA.

(D) Reactive oxygen species (ROS) release in primary neutrophils, WT, and *GATA1* KO iNeutrophils on Day 19 after treatment with DMSO, 10 nM PMA, or 10 nM PMA + 30 μM sotrastaurin. Values are presented as fold-change of mean fluorescent intensity relative to DMSO-treated cells (n = at least 3 independent experiments and 3 independent donors; mean ± SD). ****p < 0.0001, *p < 0.05 determined by two-way ANOVA.

The WT and *GATA1* KO iNeutrophils were able to phagocytose human serum opsonized fluorescent microspheres *in vitro;* however, uptake in the WT cells was reduced relative to the *GATA1* KO cells (22 ± 8% vs. 41 ± 14%, respectively). While the *GATA1* KO iNeutrophils exhibited slightly lower phagocytosis relative to the primary neutrophils (46 ± 29%), the *GATA1* KO iNeutrophils were less variable. As expected, baseline phagocytosis was inhibited in all groups after treatment with the actin polymerization inhibitor cytochalasin D (Figures 4A and 4B).

The *GATA1* KO iNeutrophils retained their MPO activity to the same degree as WT iNeutrophils, but at elevated levels relative to primary neutrophils (Figure 4C). Additionally, WT and *GATA1* KO iNeutrophils along with primary neutrophils generated baseline ROS and were further stimulated through treatment with 10 nM PMA. As expected, ROS production was inhibited with the selective protein kinase C (PKC) inhibitor sotrastaurin in all groups (Figure 4D).

GATA1 KO iNeutrophils form NETs like primary neutrophils

The formation of NETs was assessed in the WT and *GATA1* KO iNeutrophils after stimulation with PMA, the calcium ionophore A23187, and the bacterial toxin LPS. These stimulants were chosen because they induce NETs using diverse pathways. Treatment with 50 nM PMA stimulated NETs in similar numbers of WT (50 ± 5%), *GATA1* KO iNeutrophils (51 ± 13%), and primary neutrophils (67 ± 4%). Similarly, A23187 was able to induce NETs in both WT and *GATA1* KO iNeutrophils, while WT iNeutrophils produced more NETs after stimulation (83 ± 4%) compared to both *GATA1* KO iNeutrophils (62 ± 6%) and primary neutrophils (51 ± 8%) (Figures 5A and S5A). Considering both PMA and A23187 also generate extracellular traps (ETs) in other granulocytes, and flow cytometry determined that only 12 ± 2% of the WT iNeutrophils were co-positive for the neutrophil surface proteins tested, the large number of ETs seen in the WT iNeutrophils could be a product of non-neutrophil stimulation.[35,36]

While LPS is a well-described, physiologically relevant NET stimulant, it failed to induce significant NET formation in WT iNeutrophils (17 ± 12%) relative to DMSO controls (6 ± 1%), highlighting a severe limitation with this cell model. Importantly, we observed that *GATA1* KO addresses this gap through restoring sensitization to LPS and generating significant NETs (72 ± 14%) relative to DMSO controls (17 ± 12%) (Figures 5A and 5B).

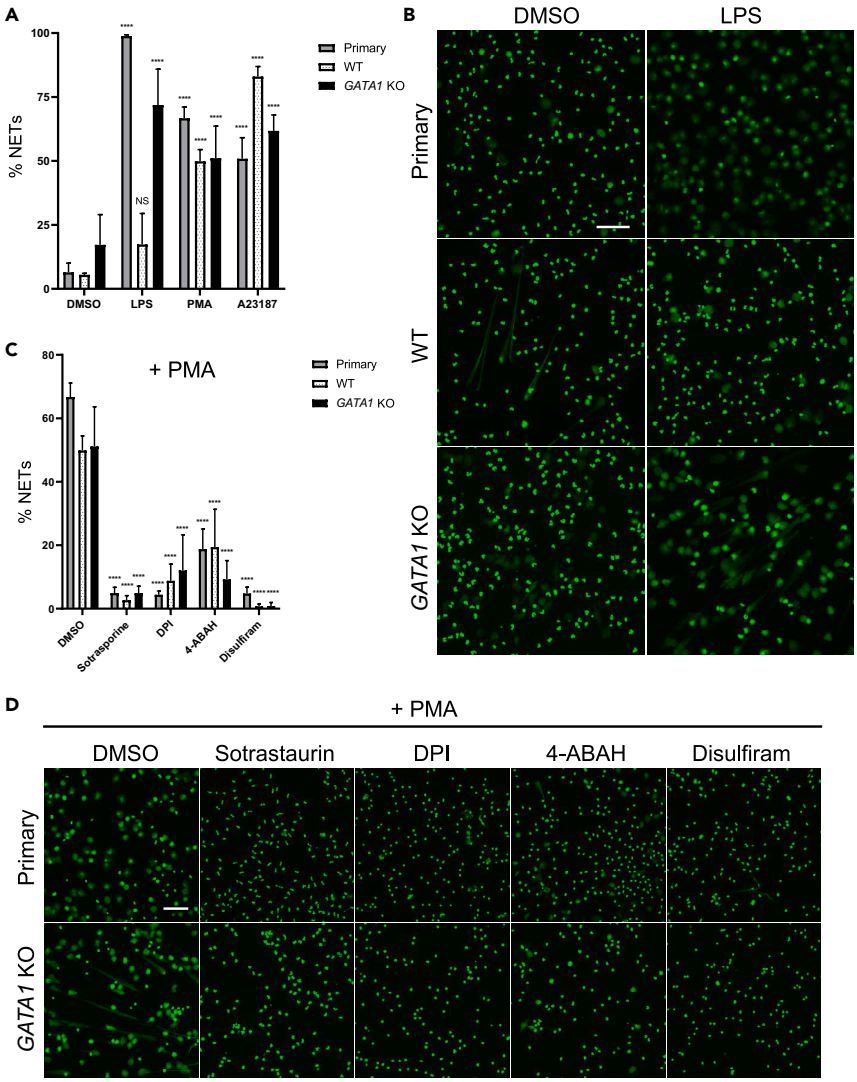

Figure 5. *GATA1* KO iNeutrophils form NETs like primary neutrophils

(A) Percentage of primary neutrophils, WT, and *GATA1* KO iNeutrophils undergoing NET formation after 3 h treatment with DMSO, 25 μg/mL LPS, 50 nM PMA, or 5 μM A23187 on Day 19 (n = at least 3 independent experiments and 3 independent donors; mean ± SD). ****p < 0.0001 as compared to unstimulated DMSO controls determined by two-way ANOVA.

(B) Fluorescent confocal microscopy of primary neutrophils', WT, and *GATA1* KO iNeutrophils' nuclei (green) after treatment with DMSO or 25 μg/mL LPS for 3 h on Day 19. Scale bar, 100 μm.

(C) Percentage of primary neutrophils, WT, and *GATA1* KO iNeutrophils undergoing NET formation after 1 h pre-incubation with DMSO, 20 μM sotrastaurin, 20 μM DPI, 100 μM 4-ABAH, or 20 μM disulfiram followed by 3 h of stimulation with 50 nM PMA on Day 19 (n = at least 3 independent experiments and 3 independent donors; mean ± SD). ****p < 0.0001 as compared to PMA-stimulated cells without inhibition determined by two-way ANOVA.

(D) Fluorescent confocal microscopy of primary neutrophils' and *GATA1* KO iNeutrophils' nuclei (green) after 1 h pre-incubation with DMSO, 20 μM sotrastaurin, 20 μM DPI, 100 μM 4-ABAH, or 20 μM disulfiram followed by 3 h of stimulation with 50 nM PMA on Day 19. Scale bar, 100 μm.

NET formation can be inhibited in *GATA1* KO iNeutrophils using small molecules as in primary neutrophils

While PMA is non-physiologic, it is a commonly used tool to study NETs *in vitro* because it reliably activates relevant pathways.[37] Like many physiologic NET-forming stimulants, PMA activates PKC and subsequently generates ROS through the NADPH oxidase (NOX) complex. This releases MPO which helps decondense chromatin and expel DNA into the extracellular environment through the pore-forming protein gasdermin D.[38–40] We investigated the fidelity of this pathway in the WT and *GATA1* KO iNeutrophils using the PKC inhibitor sotrastaurin, the NOX inhibitor diphenylene iodonium, the MPO inhibitor 4-aminobenzoic acid hydrazide, and the proposed gasdermin D inhibitor disulfiram. In line with primary neutrophils, NET formation in both the WT and *GATA1* KO iNeutrophils was significantly reduced after pre-treatment with these selective inhibitors (Figures 5C, 5D, and S5B). These results demonstrate that the *GATA1* KO iNeutrophils respond to known NET inhibitors and can be used in screens to find novel small-molecule NET inhibitors.

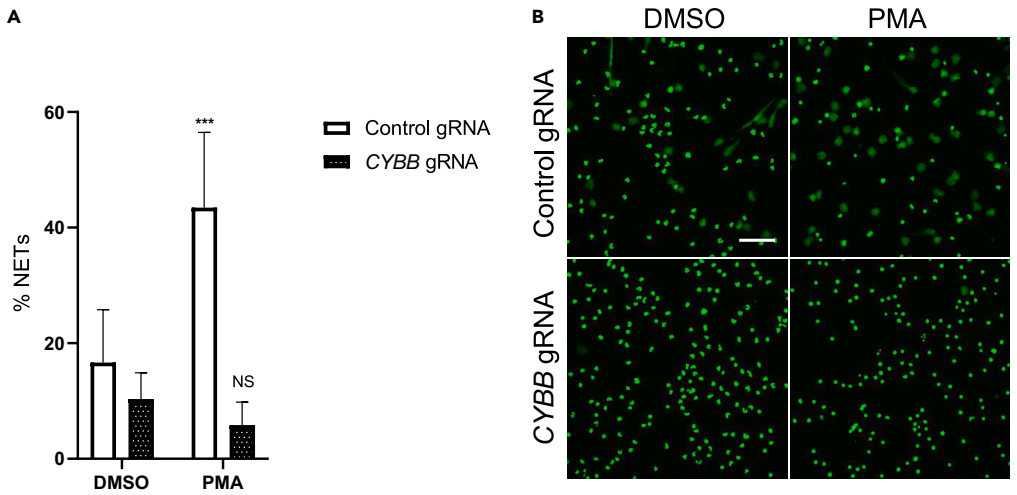

Figure 6. NET target validation in *GATA1* KO iNeutrophils

(A and B) Percentage of non-targeting (control gRNA) and *CYBB* gRNA lentiviral-transduced *GATA1* KO iNeutrophils undergoing NET formation after 3 h of treatment with DMSO or 50 nM PMA on Day 19 (n = at least 4 independent experiments; mean ± SD). ***p < 0.001 as compared to unstimulated DMSO controls determined by two-way ANOVA (B) Fluorescent confocal microscopy of control gRNA and *CYBB* gRNA lentiviral-transduced *GATA1* KO iNeutrophils' nuclei (green) after stimulation with DMSO or 50 nM PMA for 3 h. Scale bar, 100 μm.

GATA1 KO iNeutrophils can be genetically edited and used for target validation

CYBB encodes $p91^{phox}$, a component of the multi-protein NADPH complex that is critical for NOX-dependent NET formation.[37,41] To test whether *GATA1* KO iNeutrophils could be leveraged for functional genomic approaches, we knocked out *CYBB* using CRISPR-Cas9 in the *GATA1* KO hESCs, differentiated the cells to Day 19 iNeutrophils, and stimulated the cells with PMA to induce NETs. Upon stimulation with PMA, 44 ± 13% of *GATA1* KO iNeutrophils with intact $p91^{phox}$ (control gRNA) generated NETs compared to 6 ± 4% without $p91^{phox}$ (Figures 6A and 6B). These results establish that our *GATA1* KO iNeutrophils form NETs with diverse stimuli like primary neutrophils, and that NET formation can be inhibited pharmacologically and genetically. We conclude that *GATA1* KO iNeutrophils overcome a major limitation associated with primary neutrophils, by enabling the identification and validation of targets modulating neutrophil functions.

DISCUSSION

In this study, we developed a novel method that dramatically increases the efficiency of differentiation, maturity, and functionality of hPSC-derived neutrophils. Our method was adapted from previously published protocols to generate hematopoietic progenitors, with the addition of G-CSF between Day 12 and 18 to establish a granulocyte program, generating WT iNeutrophils. Recent reports optimizing the generation of iNeutrophils utilize gene overexpression to overcome differentiation challenges and deficiencies in host defense function.[21,22] Overexpression and modification of genes can enhance iNeutrophil behavior *in vitro*, but strays from primary neutrophils in ways that may not be readily apparent. These methods also require genetic manipulation during each round of cell production, adding delivery challenges and/or FACS to purify targeted cells. Unlike these protocols, our method is amenable to engineering at the self-renewing hPSC stage where modified cells can be expanded and banked for further use.

Flow cytometry analysis of WT iNeutrophils confirmed previous observations that they are composed of two distinct populations: one characterized by an immunophenotype typical of primary neutrophils and the other of either non-neutrophil granulocytes or hematopoietic progenitors. Sorting these two populations and comparing gene expression of five granulocyte regulators revealed that the neutrophil-like population expressed low *GATA1* while the non-neutrophil population highly expressed *GATA1*.

From this observation, we hypothesized that knocking out *GATA1* in the hESCs would promote the generation of enriched populations of neutrophils. hESCs with CRISPR-Cas9 deletion of *GATA1* expressed high levels of pluripotency genes, which were lost upon differentiation, consistent with the behavior and expression changes seen in WT cells. After hematopoietic induction, levels of the hematopoietic progenitor markers *SPI1* and *GFI1* rose in the Day 6 monolayer cells. Large numbers of cells began shedding off the supporting monolayer between Day 7 and Day 8, and floating *GATA1* KO cells on Day 12 expressed significantly higher levels of neutrophil-specific genes relative to the WT control, supporting our hypothesis that *GATA1* removal encourages a neutrophil program. Granulocyte specification is tightly governed by cell fate-determining transcriptional regulators, and the downregulation of *GATA1* in the hematopoietic progenitor is critical for neutrophil specification and maturation. We theorize that when *GATA1* is removed, the cells more efficiently exit the progenitor program, and without the transcriptional opportunity to produce eosinophils or basophils, automatically establish a mature neutrophil phenotype. This is highlighted by the striking similarity in the *GATA1* KO iNeutrophils' immunophenotype relative to primary neutrophils determined by flow cytometry. Other iNeutrophil differentiation protocols generate cell populations that are roughly 50% CD11b positive, with low levels of CD66b. *GATA1* KO enhances neutrophil specification and maturation seen by greater than 95% CD11b and 90% CD66b-positive cells, with approximately

85% of floating cells co-expressing the panel of neutrophil surface proteins tested, precluding time-consuming and resource-intensive sorting. Our method therefore constitutes a substantial improvement over previously described approaches.

Prior to this study, the formation of NETs in iNeutrophils has mostly been assessed using PMA, and while PMA does robustly activate specific NET pathways, it is not a physiologic stimulant. Additionally, PMA-stimulated ETs are not unique to neutrophils and occur in eosinophils.[35,36] This suggests that PMA-stimulated ETs observed in cells made following previous iNeutrophil protocols (which generate heterogeneous granulocyte populations) could be from non-neutrophil cells. Conversely, LPS is a physiologic bacterial cell wall component known to stimulate NETs *in vitro* in primary neutrophils, and by itself does not evoke DNA release in eosinophils.[42] Furthermore, studies demonstrate differential production of ETs from neutrophils and eosinophils in human disease, stressing the mechanistic differences between the two cell types.[43] Current iNeutrophil protocols generate heterogeneous populations of different granulocytes at varying stages of maturity, and while these cells form PMA-stimulated ETs, they likely do not capture the disease-relevant nuances of neutrophil-specific NETs. The relevance of these cells in NET studies is therefore limited. The *GATA1* KO iNeutrophil model overcomes these limitations by generating highly enriched cultures of neutrophil-like cells that respond to diverse NET stimulants like their primary counterpart. This is highlighted by the restoration of NET formation after stimulation with LPS.

While screens using primary neutrophils have uncovered drugs that inhibit NET formation,[39] the targets of these drugs remain extremely challenging to pinpoint. Even if a ligand partner is discovered, this does not rule out off-target modalities. For instance, a group using the potent neutrophil elastase inhibitor GW311616A concluded neutrophil elastase is critical for NET formation.[44] Follow-up work employing selective neutrophil elastase inhibitors and knockout mice dispute these findings, suggesting GW311616A's NET inhibition mechanism is likely off-target.[45,46] Furthermore, validating targets using CRISPR-Cas9 knockouts in primary human cells is challenging due to the neutrophils' extremely short lifespan *ex vivo*, and the use of classic gene silencing techniques such as siRNA or shRNA may not be effective in neutrophils, which are rather stable and transcriptionally silent. Through the deletion of *CYBB*, we show how our iNeutrophils can provide a clean method to quickly validate targets without the uncertainty of compound off-target effects.

While targeting overactive NETs in disease is therapeutically attractive, interfering with other host defense activities like phagocytosis and ROS release leaves patients vulnerable to infections.[47,48] Because *GATA1* KO iNeutrophils retain their other host defense capabilities, NET target knockout cells can serve as a tool to address the impact on these critical functions.

In conclusion, our differentiation method overcomes the limitations of previously published protocols by generating at-scale numbers of cells that are similar to primary neutrophils in form and function. COVID-19 highlights the link between dysregulated neutrophils and disease and stresses the therapeutic benefit of inhibiting unbalanced NETs. Our improved method accurately models NETs and enables large-scale screens and target validation in ways that were impossible using previous differentiation methods or primary neutrophils.

Limitations of the study

In this study, we focus on the generation of iNeutrophils from H1 hESCs. Although there are numerous reports describing the similarities between hESCs and induced pluripotent stem cells (iPSCs), we did not test the efficacy of *GATA1* KO in generating iPSC-derived iNeutrophils.

STAR★METHODS

Detailed methods are provided in the online version of this paper and include the following:

- KEY RESOURCES TABLE
- RESOURCE AVAILABILITY
  - Lead contact
  - Materials availability
  - Data and code availability
- EXPERIMENTAL MODEL AND STUDY PARTICIPANT DETAILS
  - iNeutrophil differentiation
  - Primary neutrophil isolation
- METHOD DETAILS
  - *GATA1* KO using CRISPR/Cas9
  - Immunoblotting
  - Genetic analysis
  - Hematoxylin and eosin staining
  - Flow cytometry
  - Cell sorting
  - RT-qPCR
  - ROS production
  - Phagocytosis
  - MPO activity
  - NET formation and small molecule inhibition
  - *CYBB* gRNA virus production
  - *CYBB* knockout

- QUANTIFICATION AND STATISTICAL ANALYSIS
  - Statistical analysis

SUPPLEMENTAL INFORMATION

Supplemental information can be found online at https://doi.org/10.1016/j.isci.2023.107804.

ACKNOWLEDGMENTS

This work was enabled through the generation of CRISPR-Cas9 and gRNA plasmids by Katie Worringer and Rob Maher. Haoyuan Liu generously performed the PCR to confirm *GATA1* editing. We would also like to thank Matthias Mueller, Eric Shikatani, and Gianfranco de Pascale for their expertise in the creation of the manuscript. The automation and imaging team including Felipa Mapa, Nicholas Flannery, Nicholas Blanks, Connor Rose, Dominick Casalena, Alan Ho, Shanni Chen, and John Concannon were instrumental in operating and maintaining equipment used in this study. Gizem Rizki managed the hPSC facility where experiments were performed. This research did not receive any specific grant from funding agencies in the public, commercial, or not-for-profit sectors.

AUTHOR CONTRIBUTIONS

T.H., E.O., T.S., and D.N. designed, performed, and analyzed the experiments; M.B. developed the CellProfiler pipeline to analyze NETs; S.P., C.D., S.M., and C.A. contributed to the design of the experiments; T.H., E.O., C.A., and T.S. wrote the manuscript.

DECLARATION OF INTERESTS

All authors are (or were during their involvement in this research) employees of Novartis.

INCLUSION AND DIVERSITY

We worked to ensure gender balance in the recruitment of human subjects. We worked to ensure ethnic or other types of diversity in the recruitment of human subjects. We worked to ensure that the study questionnaires were prepared in an inclusive way. One or more of the authors of this paper self-identifies as an underrepresented ethnic minority in their field of research or within their geographical location. One or more of the authors of this paper self-identifies as a gender minority in their field of research. One or more of the authors of this paper received support from a program designed to increase minority representation in their field of research.

Received: April 17, 2023
Revised: August 4, 2023
Accepted: August 29, 2023
Published: August 31, 2023

REFERENCES

1. Brinkmann, V., Reichard, U., Goosmann, C., Fauler, B., Uhlemann, Y., Weiss, D.S., Weinrauch, Y., and Zychlinsky, A. (2004). Neutrophil Extracellular Traps Kill Bacteria. Science *303*, 1532–1535. https://doi.org/10.1126/science.1092385.
2. Segal, A.W. (2005). How neutrophils kill microbes. Annu. Rev. Immunol. *23*, 197–223. https://doi.org/10.1146/annurev.immunol.23.021704.115653.
3. Khandpur, R., Carmona-Rivera, C., Vivekanandan-Giri, A., Gizinski, A., Yalavarthi, S., Knight, J.S., Friday, S., Li, S., Patel, R.M., Subramanian, V., et al. (2013). NETs are a source of citrullinated autoantigens and stimulate inflammatory responses in rheumatoid arthritis. Sci. Transl. Med. *5*, 178ra40. https://doi.org/10.1126/scitranslmed.3005580.
4. Qi, H., Yang, S., and Zhang, L. (2017). Neutrophil Extracellular Traps and endothelial dysfunction in atherosclerosis and thrombosis. Front. Immunol. *8*, 928. https://doi.org/10.3389/fimmu.2017.00928.
5. Hu, S.C.S., Yu, H.S., Yen, F.L., Lin, C.L., Chen, G.S., and Lan, C.C.E. (2016). Neutrophil extracellular trap formation is increased in psoriasis and induces human β-defensin-2 production in epidermal keratinocytes. Sci. Rep. *6*, 31119. https://doi.org/10.1038/srep31119.
6. Grabcanovic-Musija, F., Obermayer, A., Stoiber, W., Krautgartner, W.D., Steinbacher, P., Winterberg, N., Bathke, A.C., Klappacher, M., and Studnicka, M. (2015). Neutrophil extracellular trap (NET) formation characterises stable and exacerbated COPD and correlates with airflow limitation. Respir. Res. *16*, 59. https://doi.org/10.1186/s12931-015-0221-7.
7. Muñoz, L.E., Boeltz, S., Bilyy, R., Schauer, C., Mahajan, A., Widulin, N., Grüneboom, A., Herrmann, I., Boada, E., Rauh, M., et al. (2019). Neutrophil Extracellular Traps Initiate Gallstone Formation. Immunity *51*, 443–450.e4. https://doi.org/10.1016/j.immuni.2019.07.002.
8. Arcanjo, A., Logullo, J., Menezes, C.C.B., de Souza Carvalho Giangiarulo, T.C., dos Reis, M.C., de Castro, G.M.M., da Silva Fontes, Y., Todeschini, A.R., Freire-de-Lima, L., Decoté-Ricardo, D., et al. (2020). The emerging role of neutrophil extracellular traps in severe acute respiratory syndrome coronavirus 2 (COVID-19). Sci. Rep. *10*, 19630. https://doi.org/10.1038/s41598-020-76781-0.
9. Veras, F.P., Pontelli, M.C., Silva, C.M., Toller-Kawahisa, J.E., de Lima, M., Nascimento, D.C., Schneider, A.H., Caetité, D., Tavares, L.A., Paiva, I.M., et al. (2020). SARS-CoV-2-triggered neutrophil extracellular traps mediate COVID-19 pathology. J. Exp. Med. *217*, e20201129. https://doi.org/10.1084/jem.20201129.
10. Morris, G., Bortolasci, C.C., Puri, B.K., Olive, L., Marx, W., O'Neil, A., Athan, E., Carvalho, A., Maes, M., Walder, K., and Berk, M. (2021). Preventing the development of severe COVID-19 by modifying immunothrombosis. Life Sci. *264*, 118617. https://doi.org/10.1016/j.lfs.2020.118617.
11. Huang, C., Wang, Y., Li, X., Ren, L., Zhao, J., Hu, Y., Zhang, L., Fan, G., Xu, J., Gu, X., et al. (2020). Clinical features of patients infected with 2019 novel coronavirus in Wuhan, China. Lancet *395*, 497–506. https://doi.org/10.1016/S0140-6736(20)30183-5.
12. Mokhtari, T., Hassani, F., Ghaffari, N., Ebrahimi, B., Yarahmadi, A., and Hassanzadeh, G. (2020). COVID-19 and multiorgan failure: A narrative review on potential mechanisms. J. Mol. Histol. *51*, 613–628. https://doi.org/10.1007/s10735-020-09915-3.

13. Laforge, M., Elbim, C., Frère, C., Hémadi, M., Massaad, C., Nuss, P., Benoliel, J.J., and Becker, C. (2020). Tissue damage from neutrophil-induced oxidative stress in COVID-19. Nat. Rev. Immunol. *20*, 515–516. https://doi.org/10.1038/s41577-020-0407-1.
14. Zuo, Y., Yalavarthi, S., Shi, H., Gockman, K., Zuo, M., Madison, J.A., Blair, C., Weber, A., Barnes, B.J., Egeblad, M., et al. (2020). Neutrophil extracellular traps in COVID-19. JCI Insight *5*, e138999. https://doi.org/10.1172/jci.insight.138999.
15. Janiuk, K., Jabłońska, E., and Garley, M. (2021). Significance of nets formation in COVID-19. Cells *10*, 1–12. https://doi.org/10.3390/cells10010151.
16. Adrover, J.M., Carrau, L., Daßler-Plenker, J., Bram, Y., Chandar, V., Houghton, S., Redmond, D., Merrill, J.R., Shevik, M., tenOever, B.R., et al. (2022). Disulfiram inhibits neutrophil extracellular trap formation and protects rodents from acute lung injury and SARS-CoV-2 infection. JCI Insight *7*, e157342. https://doi.org/10.1172/jci.insight.157342.
17. Sinha, S., Rosin, N.L., Arora, R., Labit, E., Jaffer, A., Cao, L., Farias, R., Nguyen, A.P., de Almeida, L.G.N., Dufour, A., et al. (2022). Dexamethasone modulates immature neutrophils and interferon programming in severe COVID-19. Nat. Med. *28*, 201–211. https://doi.org/10.1038/s41591-021-01576-3.
18. Blanter, M., Gouwy, M., and Struyf, S. (2021). Studying neutrophil function *in vitro*: Cell models and environmental factors. J. Inflamm. Res. *14*, 141–162. https://doi.org/10.2147/JIR.S284941.
19. Kaufmann, M., Schuffenhauer, A., Fruh, I., Klein, J., Thiemeyer, A., Rigo, P., Gomez-Mancilla, B., Heidinger-Millot, V., Bouwmeester, T., Schopfer, U., et al. (2015). High-throughput screening using iPSC-derived neuronal progenitors to identify compounds counteracting epigenetic gene silencing in fragile X syndrome. J. Biomol. Screen *20*, 1101–1111. https://doi.org/10.1177/1087057115588287.
20. Shinozawa, T., Kimura, M., Cai, Y., Saiki, N., Yoneyama, Y., Ouchi, R., Koike, H., Maezawa, M., Zhang, R.R., Dunn, A., et al. (2021). High-Fidelity Drug-Induced Liver Injury Screen Using Human Pluripotent Stem Cell-Derived Organoids. Gastroenterology *160*, 831–846.e10. https://doi.org/10.1053/j.gastro.2020.10.002.
21. Trump, L.R., Nayak, R.C., Singh, A.K., Emberesh, S., Wellendorf, A.M., Lutzko, C.M., and Cancelas, J.A. (2019). Neutrophils Derived from Genetically Modified Human Induced Pluripotent Stem Cells Circulate and Phagocytose Bacteria In Vivo. Stem Cells Transl. Med. *8*, 557–567. https://doi.org/10.1002/sctm.18-0255.
22. Brok-Volchanskaya, V.S., Bennin, D.A., Suknuntha, K., Klemm, L.C., Huttenlocher, A., and Slukvin, I. (2019). Effective and Rapid Generation of Functional Neutrophils from Induced Pluripotent Stem Cells Using ETV2-Modified mRNA. Stem Cell Rep. *13*, 1099–1110. https://doi.org/10.1016/j.stemcr.2019.10.007.
23. Lachmann, N., Ackermann, M., Frenzel, E., Liebhaber, S., Brennig, S., Happle, C., Hoffmann, D., Klimenkova, O., Lüttge, D., Buchegger, T., et al. (2015). Large-scale hematopoietic differentiation of human induced pluripotent stem cells provides granulocytes or macrophages for cell replacement therapies. Stem Cell Rep. *4*, 282–296. https://doi.org/10.1016/j.stemcr.2015.01.005.
24. Chang, Y., Syahirah, R., Wang, X., Jin, G., Torregrosa-Allen, S., Elzey, B.D., Hummel, S.N., Wang, T., Li, C., Lian, X., et al. (2022). Engineering chimeric antigen receptor neutrophils from human pluripotent stem cells for targeted cancer immunotherapy. Cell Rep. *40*, 111128. https://doi.org/10.1016/j.celrep.2022.111128.
25. Frenz, S., Conca, R., Hesse, S., Linder, M.I., and Klein, C. (2021). Induced Pluripotent Stem Cell-Derived Neutrophil Granulocytes - Flow Cytometry Analysis Reveals Distinct Subpopulations. Blood *138*, 3126. https://doi.org/10.1182/blood-2021-150495.
26. Bartels, M., Govers, A.M., Fleskens, V., Lourenço, A.R., Pals, C.E., Vervoort, S.J., van Gent, R., Brenkman, A.B., Bierings, M.B., Ackerman, S.J., et al. (2015). Acetylation of C/EBPε is a prerequisite for terminal neutrophil differentiation. Blood *125*, 1782–1792. https://doi.org/10.1182/blood-2013-12-543850.
27. Paul, F., Arkin, Y., Giladi, A., Jaitin, D.A., Kenigsberg, E., Keren-Shaul, H., Winter, D., Lara-Astiaso, D., Gury, M., Weiner, A., et al. (2015). Transcriptional Heterogeneity and Lineage Commitment in Myeloid Progenitors. Cell *163*, 1663–1677. https://doi.org/10.1016/j.cell.2015.11.013.
28. Bjerregaard, M.D., Jurlander, J., Klausen, P., Borregaard, N., and Cowland, J.B. (2003). The *in vivo* profile of transcription factors during neutrophil differentiation in human bone marrow. Blood *101*, 4322–4332. https://doi.org/10.1182/blood-2002-03-0835.
29. Hirasawa, R., Shimizu, R., Takahashi, S., Osawa, M., Takayanagi, S., Kato, Y., Onodera, M., Minegishi, N., Yamamoto, M., Fukao, K., et al. (2002). Essential and instructive roles of GATA factors in eosinophil development. J. Exp. Med. *195*, 1379–1386. https://doi.org/10.1084/jem.20020170.
30. Nei, Y., Obata-Ninomiya, K., Tsutsui, H., Ishiwata, K., Miyasaka, M., Matsumoto, K., Nakae, S., Kanuka, H., Inase, N., and Karasuyama, H. (2013). GATA-1 regulates the generation and function of basophils. Proc. Natl. Acad. Sci. USA. *110*, 18620–18625. https://doi.org/10.1073/pnas.1311668110.
31. Heinze, D., Park, S., McCracken, A., Haratianfar, M., Lindstrom, J., Villacorta-Martin, C., Mithal, A., Wang, F., Yang, M.W., Murphy, G., and Mostoslavsky, G. (2022). Notch activation during early mesoderm induction modulates emergence of the T/NK cell lineage from human iPSCs. Stem Cell Rep. *17*, 2610–2628. https://doi.org/10.1016/j.stemcr.2022.10.007.
32. Ditadi, A., Sturgeon, C.M., Tober, J., Awong, G., Kennedy, M., Yzaguirre, A.D., Azzola, L., Ng, E.S., Stanley, E.G., French, D.L., et al. (2015). Human definitive haemogenic endothelium and arterial vascular endothelium represent distinct lineages. Nat. Cell Biol. *17*, 580–591. https://doi.org/10.1038/ncb3161.
33. Demetri, G.D., and Griffin, J.D. (1991). Granulocyte colony-stimulating factor and its receptor. Blood *78*, 2791–2808.
34. Gutiérrez, L., Nikolic, T., Van Dijk, T.B., Hammad, H., Vos, N., Willart, M., Grosveld, F., Philipsen, S., and Lambrecht, B.N. (2007). Gata1 regulates dendritic-cell development and survival. Blood *110*, 1933–1941. https://doi.org/10.1182/blood-2006-09.
35. Ueki, S., Melo, R.C.N., Ghiran, I., Spencer, L.A., Dvorak, A.M., and Weller, P.F. (2013). Eosinophil extracellular DNA trap cell death mediates lytic release of free secretion-competent eosinophil granules in humans. Blood *121*, 2074–2083. https://doi.org/10.1182/blood-2012-05-432088.
36. Germic, N., Stojkov, D., Oberson, K., Yousefi, S., and Simon, H.U. (2017). Neither eosinophils nor neutrophils require ATG5-dependent autophagy for extracellular DNA trap formation. Immunology *152*, 517–525. https://doi.org/10.1111/imm.12790.
37. Kenny, E.F., Herzig, A., Krüger, R., Muth, A., Mondal, S., Thompson, P.R., Brinkmann, V., Bernuth, H.v., and Zychlinsky, A. (2017). Diverse stimuli engage different neutrophil extracellular trap pathways. Elife *6*, e24437. https://doi.org/10.7554/eLife.24437.
38. Hu, J.J., Liu, X., Xia, S., Zhang, Z., Zhang, Y., Zhao, J., Ruan, J., Luo, X., Lou, X., Bai, Y., et al. (2020). FDA-approved disulfiram inhibits pyroptosis by blocking gasdermin D pore formation. Nat. Immunol. *21*, 736–745. https://doi.org/10.1038/s41590-020-0669-6.
39. Sollberger, G., Choidas, A., Burn, G.L., Habenberger, P., Di Lucrezia, R., Kordes, S., Menninger, S., Eickhoff, J., Nussbaumer, P., Klebl, B., et al. (2018). Gasdermin D plays a vital role in the generation of neutrophil extracellular traps. Sci. Immunol. *3*, 6689. https://doi.org/10.1126/sciimmunol.aar6689.
40. Metzler, K.D., Fuchs, T.A., Nauseef, W.M., Reumaux, D., Roesler, J., Schulze, I., Wahn, V., Papayannopoulos, V., and Zychlinsky, A. (2011). Myeloperoxidase is required for neutrophil extracellular trap formation: Implications for innate immunity. Blood *117*, 953–959. https://doi.org/10.1182/blood-2010-06-290171.
41. Khan, M.A., Farahvash, A., Douda, D.N., Licht, J.C., Grasemann, H., Sweezey, N., and Palaniyar, N. (2017). JNK Activation Turns on LPS-And Gram-Negative Bacteria-Induced NADPH Oxidase-Dependent Suicidal NETosis. Sci. Rep. *7*, 3409. https://doi.org/10.1038/s41598-017-03257-z.
42. Yousefi, S., Gold, J.A., Andina, N., Lee, J.J., Kelly, A.M., Kozlowski, E., Schmid, I., Straumann, A., Reichenbach, J., Gleich, G.J., and Simon, H.U. (2008). Catapult-like release of mitochondrial DNA by eosinophils contributes to antibacterial defense. Nat. Med. *14*, 949–953. https://doi.org/10.1038/nm.1855.
43. Hwang, C.S., Park, S.C., Cho, H.J., Park, D.J., Yoon, J.H., and Kim, C.H. (2019). Eosinophil extracellular trap formation is closely associated with disease severity in chronic rhinosinusitis regardless of nasal polyp status. Sci. Rep. *9*, 8061. https://doi.org/10.1038/s41598-019-44627-z.
44. Papayannopoulos, V., Metzler, K.D., Hakkim, A., and Zychlinsky, A. (2010). Neutrophil elastase and myeloperoxidase regulate the formation of neutrophil extracellular traps. J. Cell Biol. *191*, 677–691. https://doi.org/10.1083/jcb.201006052.
45. Kasperkiewicz, P., Hempel, A., Janiszewski, T., Kołt, S., Snipas, S.J., Drag, M., and Salvesen, G.S. (2020). NETosis occurs independently of neutrophil serine proteases. J. Biol. Chem. *295*, 17624–17631. https://doi.org/10.1074/jbc.RA120.015682.
46. Martinod, K., Witsch, T., Farley, K., Gallant, M., Remold-O'Donnell, E., and Wagner, D.D. (2016). Neutrophil elastase-deficient mice form neutrophil extracellular traps in an

experimental model of deep vein thrombosis. J. Thromb. Haemost. *14*, 551–558. https://doi.org/10.1111/jth.13239.

47. Danikas, D.D., Karakantza, M., Theodorou, G.L., Sakellaropoulos, G.C., and Gogos, C.A. (2008). Prognostic value of phagocytic activity of neutrophils and monocytes in sepsis. Correlation to CD64 and CD14 antigen expression. Clin. Exp. Immunol. *154*, 87–97. https://doi.org/10.1111/j.1365-2249.2008.03737.x.
48. Quie, P.G., White, J.G., Holmes, B., and Good, R.A. (1967). In Vitro Bactericidal Capacity of Human Polymorphonuclear Leukocytes: Diminished Activity in Chronic Granulomatous Disease of Childhood. J. Clin. Invest. *46*, 668–679. https://doi.org/10.1172/JCI105568.
49. Bookout, A.L., Cummins, C.L., Mangelsdorf, D.J., Pesola, J.M., and Kramer, M.F. (2006). High-Throughput Real-Time Quantitative Reverse Transcription PCR. Curr. Protoc. Mol. Biol. *Chapter 15*. Unit 15.8. https://doi.org/10.1002/0471142727.mb1508s73.

STAR★METHODS

KEY RESOURCES TABLE

REAGENT or RESOURCE	SOURCE	IDENTIFIER
Antibodies		
Anti-CD33	BioLegend	Cat# 366605, RRID:AB_2565753
Anti-CD45	BioLegend	Cat# 368508, RRID:AB_2566368
Anti-CD15	BD Biosciences	Cat# 563141, RRID:AB_2738025
Anti-CD66b	eBioscience	Cat# 25-0666-42, RRID:AB_2573360
Anti-CD11b	BD Biosciences	Cat# 561690, RRID:AB_10897015
Anti-CD16	BD Biosciences	Cat# 557758, RRID:AB_396864
Anti-CD182	BioLegend	Cat# 320705, RRID:AB_439806
Anti-CD193	BioLegend	Cat# 310705, RRID:AB_345395
Anti-CD49d	BioLegend	Cat# 304315, RRID:AB_2561758
Anti-Siglec-8	BioLegend	Cat# 347105, RRID:AB_2561401
Anti-GATA1	Invitrogen	Cat# 700727, RRID:AB_2532341
Anti-ß-Actin	Sigma-Aldrich	Cat# A5441, RRID:AB_2561401
Chemicals, peptides, and recombinant proteins		
hESC Matrigel	Corning	Cat# 354277
Hematopoietic Matrigel	Corning	Cat# 354234
Y-27632	Tocris	Cat# 1254
aMTG	Sigma-Aldrich	Cat# M6145
Transferrin	Sigma-Aldrich	Cat# 10652202001
L-Ascorbic Acid	Sigma-Aldrich	Cat# A4403
BMP4	R&D Systems	Cat# 314-BP
VEGF	R&D Systems	Cat# 293-VE
CHIR99021	Tocris	Cat# 4423
bFGF	R&D Systems	Cat# 233-FB
IL-6	R&D Systems	Cat# 206-IL
Flt3L	PeproTech	Cat# 300-19
IL-11	PeproTech	Cat# 200-11
IGF-1	R&D Systems	Cat# 291-G1
IL-3	R&D Systems	Cat# 203-IL
TPO	PeproTech	Cat# 300-18
SCF	R&D Systems	Cat# 255-SC
SSH	PeproTech	Cat# 100-45
Angiotensin II	Sigma-Aldrich	Cat# A9525
G-CSF	PeproTech	Cat# 300-23
PMA	Sigma-Aldrich	Cat# P1585
LPS O128:B12	Sigma-Aldrich	Cat# L2887
A23187	Sigma-Aldrich	Cat# C7522
Sotrastaurin	Selleck Chemicals	Cat# S2791
DPI	Sigma-Aldrich	Cat# D2926
4-ABAH	Sigma-Aldrich	Cat# A41909
Disulfiram	Tocris	Cat# 3807

(*Continued on next page*)

Continued

REAGENT or RESOURCE	SOURCE	IDENTIFIER
Critical commercial assays		
hESC Genetic Analysis Kit	StemCell Tech	Cat# 07550
General Oxidative Stress Indicator Kit	Invitrogen	Cat# C6827
EnzChek Myeloperoxidase Activity Assay Kit	Invitrogen	Cat# E33856
Experimental models: Cell lines		
H1 human embryonic stem cells	WiCell	Cat# WAe001-A
Software and algorithms		
FlowJo V10.7.1	FlowJo, LLC	FlowJo, RRID:SCR_008520
CellProfiler 4.2.4	Broad Institute	CellProfiler, RRID:SCR_007358
GraphPad Prism 9	Dotmatics	GraphPad Prism, RRID:SCR_002798

RESOURCE AVAILABILITY

Lead contact

Further information and requests for resources and reagents should be directed to and will be fulfilled by the lead contact, Thomas C. Harper (tomdomma@gmail.com).

Materials availability

There are restrictions to the availability of the cell lines used due to MTA limitations.

Data and code availability

- All data reported in this paper will be shared by the lead contact upon request
- This paper does not report original code
- Any additional information required to reanalyze the data reported in this paper is available from the lead contact upon request

EXPERIMENTAL MODEL AND STUDY PARTICIPANT DETAILS

iNeutrophil differentiation

Differentiation was adapted from previously published protocols.[31,32] Both Cas9 expressing WT and Cas9 expressing *GATA1* KO hESCs were cultured in humidified tissue culture incubators at 37°C with 5% $C0_2$. Cells were maintained on Matrigel (Corning, 354277) coated dishes using mTeSR Plus media (StemCell Tech, 100-0276). The day before induction (Day -1), cells were dissociated into 100 to 300 μm clumps using ReLeSR (StemCell Tech, 05872) and 6 $x10^4$ cells were plated onto hematopoietic Matrigel (Corning, 354234) coated 6 cm dishes in mTeSR Plus media with 10 μM Y-27632 (Tocris, 1254). Cell numbers were determined by dissociating un-plated clumps into single cells using TrypLE Express (Invitrogen, 12605010) and quantified using a Luna FL cell counter (Logos Biosystems, L20001). On Day 0, mTeSR Plus was removed and cells were induced with Base Media 1 (StemPro 34 SFM Media (Gibco, 10639011) containing 1x GlutaMAX (Gibco, 35050079), 0.45 mM aMTG (Sigma-Aldrich, M6145), 200 μg/ml Transferrin (Sigma-Aldrich, 10652202001), and 88 μg/ml L-Ascorbic Acid (Sigma-Aldrich, A4403) supplemented with 5 ng/ml BMP4 (R&D Systems, 314-BP), 50 ng/ml VEGF (R&D Systems, 293-VE) and 2 μM CHIR99021 (Tocris, 4423). Cells were incubated for two days. On Day 2, cells were refreshed with Base Media 1 plus 5 ng/ml BMP4, 50 ng/ml VEGF, and 20 ng/ml bFGF (R&D Systems, 233-FB). On Day 4, cells were again refreshed with Base Media 1 plus 15 ng/ml VEGF and 5 ng/ml bFGF. On Day 6, media was replaced with Base Media 2 (StemPro 34 SFM Media containing 1x GlutaMAX, 0.4 mM aMTG, 150 μg/ml Transferrin, and 50 μg/ml L-Ascorbic Acid)) supplemented with Growth Factor Cocktail (5 ng/ml BMP4, 5 ng/ml bFGF, 10 ng/ml IL-6 (R&D systems, 206-IL), 10 ng/ml Flt3L (PeproTech, 300-19), 5 ng/ml IL-11 (PeproTech, 200-11), 25 ng/ml IGF-1 (R&D Systems, 291-G1), 30 ng/ml IL-3 (R&D Systems, 203-IL), 30 ng/ml TPO (PeproTech, 300-18), 50 ng/ml VEGF, 100 ng/ml SCF (R&D Systems, 255-SC), 20 ng/ml SHH (PeproTech, 100-45) and 10 μg/ml Angiotensin II (Sigma-Aldrich, A9525)). After one or two days, cells began to shed away from the adherent monolayer, so during each media change, used media containing floating cells was collected, centrifuged at 300 x g for 10 minutes to pellet cells, resuspended in fresh media, and returned to their original dishes. Media was changed every other day using Base Media 2 plus Growth Factor Cocktail until Day 12, when floating cells were collected and plated into new 6 cm dishes with Maturation Media (RPMI (Gibco, 61870036), 10% FBS, 1 mM Sodium Pyruvate (Gibco, 11360070), 55 μM 2-Mercaptoethanol (Gibco, 21985023), 25 mM HEPES (Gibco, 15630130), and 100 ng/ml G-CSF (PeproTech, 300-23)). Maturation Media was changed every other day until Day 18 when G-CSF was removed for 24 hours before experiments on Day 19 to avoid G-CSF related stimulation. At harvest, cells were strained through a 15 μm filter (pluriSelect, 43-50015-03) to remove debris followed by centrifugation for 10 minutes at 300 x g to pellet cells. Cell numbers were quantified using a Beckman Coulter Vi-Cell XR cell viability analyzer.

Primary neutrophil isolation

Peripheral blood from healthy donors (defined as not having asthma or allergies and not having taken NSAIDS within the previous 5 days) was obtained at Novartis Institutes of Biomedical Research using informed consent under an approved Institutional Review Board research protocol. Fresh blood was EDTA anti-coagulated and used within two hours of donation. Primary donor neutrophils were extracted using Ficoll-density centrifugation. Per 10 ml of fresh blood, 5 ml of PBS and 5 ml of 4% Dextran (Sigma-Aldrich, 31392-50G) in PBS (Gibco, 10010-023) were added and mixed in a 50 ml tube by gently by inverting 2.5 times, then allowed to settle for 30 minutes at room temperature, separating into a dense layer topped with a supernatant containing leukocytes. 75% of the supernatant volume of Ficoll-Paque Premium (Sigma-Aldrich, GE17-5442-03) was added to a new 50 ml falcon tube. The supernatant was carefully transferred on top of the Ficoll, then centrifuged at 650 x g for 20 minutes at room temperature, with a low acceleration (2) and no brake (deceleration set to 0). The supernatant was removed, then the pellet was resuspended in 10 ml of water (Ultrapure diH2O) and mixed no more than 30 seconds to lyse red blood cells. Then 10 ml of 2 x PBS (made from 10 x PBS Gibco, 70011044) was added, and tubes were centrifuged 300 x g for 10 minutes at room temperature (reset acceleration and deceleration to 9). The supernatant was aspirated, and the pellet containing granulocytes was resuspended in IMDM (Gibco, 21056023) and counted with a ViCell Cell Counter. For the ROS assay, primary neutrophils were resuspended in Hanks Balanced Salt Solution (HBSS, Gibco, 14025-092) and counted.

METHOD DETAILS

GATA1 KO using CRISPR/Cas9

An Amaxa Nucleofector II Device and Nucleofector Kit (Lonza, VPH-5012) were used to transiently express 5 μg of *GATA1* gRNA plasmid (gRNA sequence: GGTGTGGAGGACACCAGAGC) containing a puromycin resistance gene into 1 x 10^6 WT H1 hESCs constitutively expressing *Cas9* from the *AAVS1* locus. After nucleofection, cells were plated onto a 6 cm dish in mTeSR plus media with 10 μM Y-27632, and two days later selected using 1 μg/ml puromycin for 2 days, clonally expanded, genomic DNA extracted (Invitrogen, K1820-1), and target locus PCR amplified (forward primer: GATGCAGGAGGGAAAAGAGAGGA, reverse primer: GCAACCACCACATACTTCCAGT) using Platinum *Taq* DNA Polymerase (Invitrogen, 11304011). Amplicons were analyzed using Sanger sequencing and clones with frame shift deletions picked for expansion. All experiments were performed using a *GATA1* KO clone containing a 13 base-pair frame shift deletion with confirmed GATA1 protein loss determined by western blot (Figures S1A and S1B). *GATA1* is located on the X-chromosome so only one allele of H1 hESCs (XY karyotype) required editing.

Immunoblotting

5 x 10^6 Day 19 WT and *GATA1* KO iNeutrophils were lysed in RIPA buffer (Invitrogen, 89900) containing HALT protease inhibitor cocktail (Invitrogen, 78429). Protein concentrations were quantified using a Direct Detect Spectrometer (Millipore Sigma, C134681) and normalized in NuPAGE LSD Sample Buffer (Invitrogen, NP0007) and NuPAGE Sample Reducing Agent (Invitrogen, NP0009) followed by incubation at 70°C for 10 minutes. Samples were distributed into a NuPAGE Novex 4-12% Bis-Tris Gel (Invitrogen, NP0321BOX) and loaded into an XCell SureLock Mini-Cell (Invitrogen, EI0001) containing NuPAGE MOPS SDS Running Buffer (Invitrogen, NP0001). After 1.5 hours of electrophoresis, samples were transferred to a Trans-Blot Turbo Nitrocellulose Membrane (Bio-Rad, 1704159). Membranes were blocked in TBST (Invitrogen, J77500.K2) with 3% skim milk for 1 hour at room temperature followed by overnight incubation at 4°C with rabbit anti-GATA1 (Invitrogen, 700727) or mouse anti-ß-Actin (Sigma-Aldrich, A5441) in TBST with 3% skim milk. Membranes were washed 3 x in TBST followed by incubation with either HRP anti-rabbit (Cytiva, NA934) or HRP anti-mouse (Cytiva, NA931) secondary antibodies in TBST with 3% skim milk at room temperature for one hour.

Genetic analysis

After *GATA1* deletion, chromosomal copy numbers were analyzed using the hPSC Genetic Analysis Kit (StemCell Tech, 07550) following the manufacture's protocol. Briefly, WT and *GATA1* KO hESC DNA were harvested and analyzed using qPCR to detect eight of the most common karyotypic abnormalities reported in hPSCs. Both the WT and *GATA1* KO cells displayed expected numbers of assayed chromosomes relative to a normal karyotype control (Figure S2).

Hematoxylin and eosin staining

To visualize morphology, 1.5 x 10^5 cells were suspended in 200 μl PBS plus 1% BSA (Sigma-Aldrich, A9576) and spun onto glass slides using a Thermo Scientific Cytospin 4 centrifuge at 300 x g for 5 minutes, processed through a Siemens Hematek 2000 for staining and sealed / preserved using DPX mounting media (Sigma-Aldrich, 06522). Stained cells were then visualized using a Nikon Eclipse Ci-L microscope.

Flow cytometry

5 x 10^5 cells per condition were distributed into a 96 well v-bottom plate (Corning, 3357), washed with stain buffer (BD Biosciences, 554657), then incubated with 200 μl fluorophore-conjugated antibodies diluted in stain buffer for 30 minutes on ice. Cells were then washed two times and fixed with 4% paraformaldehyde (Electron Microscopy Services, 15710) diluted in PBS for 30 minutes followed by two more washes. For washes, 200 μl of stain buffer were added to each sample well followed by centrifugation at 300 x g for 5 minutes at 4°C. All steps were performed in dark conditions and on ice. Antigen specific antibodies reacted to UltraComp eBeads (Invitrogen, 01-3333-42) were used as

single-color compensation controls and corresponding isotype controls were included for each antigen specific antibody. Experiment was run using a Yeti (Propel Labs) flow cytometer and analysis was performed using FlowJo software. To calculate positive marker expression, a cut off of no more than 3% isotype background was used. Experiment was performed on three independent differentiations and one independent donor.

Cell sorting

10 x 10^6 Day 19 WT iNeutrophils were resuspended in 4 ml PBS + 1% BSA (Sigma-Aldrich, A9576) and sorted using a FACSAria III (BD Biosciences) based on low and high forward- and side-scatter populations gated in Figure 1D. Once sorted, the two populations were immediately processed for RT-qPCR.

RT-qPCR

Approximately 2 x 10^6 cells were harvested, and RNA extracted and purified using the RNeasy Mini Kit (Qiagen, 74104), reverse transcribed using SuperScript IV Reverse Transcriptase (Invitrogen, 18090010), and gene expression analyzed by TaqMan assay using Fast Advanced Master Mix (Applied Biosystems, 4444963) and the QuantStudio Flex Real-Time PCR System (Applied Biosystems, 4485701). Fold-changes relative to WT H1 hESCs were calculated using the delta-delta Ct method and normalized using the housekeeping gene *GAPDH* and experimental error was calculated through standard deviation.[49] For the time-course study, samples were collected from three independent differentiations and performed in technical triplicates. TaqMan probes used are listed in Table S1.

ROS production

ROS release was measured using the CM-H2DCFDA (General Oxidative Stress Indicator) kit (Invitrogen, C6827) following the manufacturer's protocol. Briefly, cells were resuspended to 1x10^6 cells/ml in warm Hanks Balanced Salt Solution (HBSS, Gibco, 14025-092) with 5 μM CM-H2DCFDA dye, incubated at 37°C for 20 minutes, then washed with HBSS. Sotrastaurin was transferred to black-walled, clear-bottomed 384 well cell plates (Greiner, 781091) using the LabCyte Echo for a final concentration of 30 μM, then 2.5 x10^4 cells / well were added directly into plates and pre-treated for 30 minutes at 37°C. Plates were washed with HBSS, then treated with 10 nM PMA stimulant or DMSO for one hour at 37°C. Fluorescence of 2',7'-dichlorofluorescein generated by ROS-induced oxidation of the DCFDA reagent to was measured on a CLARIOstar plate reader at 488 / 535 excitation / emission, then adjusted down by 75% of highest well to bring all wells into range. Mean fluorescence from cell-free wells was subtracted to control for background fluorescence. Experiment was performed on four independent differentiations and three independent donors in at least five technical replicates per experiment.

Phagocytosis

Primary neutrophils or iNeutrophils were seeded in V-bottom 96 well plates (Greiner, 651201) at 5 x 10^5 cells / well in 100 μl of IMDM (Gibco, 21056023), then treated with either DMSO or 20 μM cytochalasin D (Sigma-Aldrich, C8273) and incubated at 37°C for 1 hour. During the incubation, 500 μl of Fluoresbrite YG Carboxylate Microspheres 1.75 μm (PolySciences, 17687-5) were opsonized in 4500 μl of Normal Human Serum (GeminiBio, 100-110) diluted 50 / 50 in PBS. Fluorescent particles were incubated at room temperature in the dark for 5 minutes then spun down at 300 x g. The supernatant was removed and the opsonization process was repeated one more time. After the second spin the beads were resuspended in 5 ml of 50 / 50 normal human serum / PBS mixture and 100 μl of the opsonized beads were added per well and incubated for 30 minutes at 37°C. After incubation, the cells were spun down at 300 x g in a 4°C centrifuge and the supernatant was removed. Cells were fixed for 5 minutes with 100 μl / well 4% paraformaldehyde in PBS, then washed twice with ice-cold PBS. After the second wash the supernatant was removed and 200 μl of PBS, followed by 100 μl of 0.4% trypan blue, was added to each well. Cells were then analyzed by flow cytometry for uptake of fluorescent particles. Experiment was performed on at least three independent differentiations and three independent donors in at least technical triplicates.

MPO activity

The MPO activity of cell lysates was measured using an EnzChek Myeloperoxidase Activity Assay Kit (Invitrogen, E33856) following manufacturer's instructions. Briefly, cells were resuspended in at 5 x 10^5 cells / ml in PBS and lysed through freeze thaw cycles and 25 μl added to each well of a 384 well dish (PerkinElmer, 6007270). Chlorination was measured by addition of AFP reagent and fluorescence was measured using a BMG PHERAstar at excitation and emission wavelengths of 485 nm and 520 nm, respectively. Mean fluorescence from cell-free wells was subtracted from experiment wells to control for background fluorescence. Experiments were performed on three independent differentiations and three independent donors using at least technical triplicates.

NET formation and small molecule inhibition

WT iNeutrophils, *GATA1* KO and primary neutrophils were plated in IMDM (Gibco, 21056023) at a density of 5 x 10^4 cells per well in ultra-low base 384 well dishes (Aurora, ABD241001A) and stimulated using 50 nM PMA (Sigma-Aldrich, P1585), 25 μg/ml LPS O128:B12, (Sigma-Aldrich, L2887) or 5 μM A23187 (Sigma-Aldrich, C7522) for 3 hours at 37°C. For inhibition studies, cells were pre-treated with 20 μM sotrastaurin (Selleck Chemicals, S2791), 20 μM DPI (Sigma-Aldrich, D2926), 100 μM 4-ABAH (Sigma-Aldrich, A41909) or 20 μM disulfiram (Tocris, 3807) for 1 hour followed by 3 hours of stimulation using 50 nM PMA. After the 3 hour stimulation, a fix/perm/stain solution was added for a final

concentration of 2% paraformaldehyde (Electron Microscopy Services, 15710), 0.1% Triton X100 (Sigma-Aldrich, X100-100ML) and 50 nM Sytox Green (Invitrogen, S7020). Nine fields per well were imaged using the Yokogawa CV8000 automated microscope at 20x magnification. Image features were extracted using CellProfiler followed by analysis using custom supervised machine learning software to classify NET versus non-NET nuclei based on nuclei features including size, shape, intensity, etc. Experiments were performed on at least three independent differentiations and three independent donors in at least technical triplicates.

CYBB gRNA virus production

Lentiviral particles coding for a gRNA against CYBB and a non-targeting control were generated using standard procedures. Briefly, 10 cm dishes of 95% confluent 293FT cells (Invitrogen, R70007) were transfected with 2 μg transfer vector containing gRNAs (CYBB gRNA: TTGGCGATCTCAACAGAAGG, non-targeting control gRNA: GTAGCGAACGTGTCCGGCGT) and puromycin resistance genes along with 5 μg of Lentiviral Packaging Plasmid Mix (Cellecta, CPCP-K2A) using Lipofectamine 3000 (Invitrogen, L3000001), Opti-MEM media (Invitrogen, 31985062) and 3% FBS. 12 hours post-transfection, media was replaced with DMEM 1X (Invitrogen, 11995040) containing 10% FBS. Supernatants were then collected after 48 and 72 hours, pooled, and centrifuged at 1000 x g for 10 minutes at 4°C to pellet debris. Supernatants were then filtered through a 0.45 μm filter (Corning, 431155) and concentrated using Lenti-X Concentrator (Takara, 631232) using the manufacturer's instructions.

CYBB knockout

GATA1 KO hESCs were cultured in a Matrigel coated 6 well tissue culture dish in mTeSR Plus media. When cells reached approximately 25% confluency, 50 μl *CYBB* and control gRNA virus was added to separate wells for 24 hours followed by a complete media change. 48 hours post transduction, virally integrated cells were selected for using 1 μg/ml puromycin. Cells were cultured in selection media for at least 1 week prior to experimentation.

QUANTIFICATION AND STATISTICAL ANALYSIS

Statistical analysis

Data in this study was analyzed, compared and graphed using GraphPad Prism. Unpaired, two-tailed Student's t-tests were used when comparing two groups. For comparison between multiple groups, either a one-way or two-way ANOVA was performed followed by Bonferroni's multiple comparison test. Biological replicates are noted in figure legends. Statistical significance was set at $p < 0.05$. Asterisks represent the following: *$p < 0.05$, **$p < 0.01$, ***$p < 0.001$ and ****$p < 0.0001$.